JOURNAL OF SOLID STATE CHEMISTRY 64, 188–199 (1986)

The Structure and Properties of $Li_{1-x}H_xNbO_3$

C. E. RICE

AT&T Bell Laboratories, Murray Hill, New Jersey 07974

Received October 21, 1985; in revised form January 24, 1986

The properties of $Li_{1-x}H_xNbO_3$ have been studied as a function of x, temperature, and stoichiometry of the $LiNbO_3$ used for its preparation. X-ray diffraction, thermal analysis measurements, and infrared spectroscopy have been used. The intent of this study was to gain a deeper understanding of the basic properties of this material, which has potential importance as a waveguide material in $LiNbO_3$ optical devices. An approximate phase diagram was constructed for the stoichiometric $LiNbO_3$–$HNbO_3$ system. In one concentration range ($0.56 \leq x \leq 0.75$), particularly complex structural behavior was found: depending on x, samples undergo one, two, or three phase transitions with temperature, and the system appears to exhibit critical behavior. Samples made by proton exchange of congruent $LiNbO_3$ ($[Li_2O]_{0.486}[Nb_2O_5]_{0.514}$) show generally similar structural chemistry, with one exception: a new monoclinic phase, isomorphous with MnF_3, was found for $0.75 \leq x \leq 0.77$. Possible reasons for the refractive index changes caused by proton exchange are discussed.

Introduction

We have reported that $LiNbO_3$ (as well as $LiTaO_3$) undergoes ion exchange in acidic media, replacing some or all of the lithium ions with protons (*1*). This process, which we have called proton exchange (PE), is unusual and unexpected, the lithium ion mobility in these compounds being quite low at exchange temperatures. Partially exchanged $LiNbO_3$ is of particular interest, since proton substitution produces large changes in the refractive indices: the extraordinary index n_e increases by 0.12 while the ordinary index n_o decreases by 0.05 (at 633 nm) (*2*). A great deal of study has taken place, both in our laboratory and elsewhere, concerning the fabrication and behavior of PE $LiNbO_3$ waveguides and devices (*3*). However, much remains unknown about the basic properties of this material.

We have recently published a preliminary study (*4*) of the structural behavior of rhombohedral $Li_{1-x}H_xNbO_3$ as a function of proton concentration and thermal history, using stoichiometric $LiNbO_3$ as a starting material. In that work, all structural data were obtained at room temperature. This paper presents an expanded study of the properties of proton-substituted materials prepared from both stoichiometric and congruent-melting $LiNbO_3$ ($[Li_2O]_{0.486}[Nb_2O_5]_{0.514}$, the material commercially available as single crystals for device fabrication). These properties were studied using X-ray diffraction as a function of composition and temperature, thermal measurements, and infrared spectroscopy. The results provide a more detailed under-

0022-4596/86 $3.00

standing of this system, and reveal a complex and unusual structural chemistry.

Experimental

Synthesis. Stoichiometric $LiNbO_3$ (Herman C. Starck, Berlin) had a particle size of ~1–5 μ, and was used as received. Analysis results (all analyses were performed by Schwarzkopf Microanalytical Laboratories): $[Li_2O]_{0.501}[Nb_2O_5]_{0.499}$. Congruent $LiNbO_3$ (Johnson-Matthey) was ground and sieved to 635 mesh (~20 μ). Analyzed: $[Li_2O]_{0.483}[Nb_2O_5]_{0.517}$.

The preparation of the PE stoichiometric $LiNbO_3$ has been described in Ref. (*4*); congruent $Li_{1-x}H_xNbO_3$ samples were prepared for x = 0.59, 0.65, 0.73, 0.75, 0.76, 0.77, 0.81, and 0.90 by exchange in lithium benzoate/benzoic acid melts in a similar fashion, but for longer times (up to 600 hr) because of the larger particle size. The latter samples were analyzed for hydrogen and lithium. In all cases, hydrogen was found to replace lithium on a one-for-one basis. For simplicity, all exchanged samples will be referred to as either stoichiometric or congruent $Li_{1-x}H_xNbO_3$ (or PE $LiNbO_3$), with the understanding that the congruent samples are actually $[(Li_2O)_{1-x}(H_2O)_x]_{0.486}[Nb_2O_5]_{0.514}$. The variation of x in $Li_{1-x}H_xNbO_3$ as a function of melt composition is shown in Fig. 1.

Structural characterization. X-ray diffraction data were collected on a Scintag diffractometer using CuK_α radiation. Tungsten powder was used as an internal standard. For data collection above room temperature, samples were mounted on a tin oxide-coated glass slide using a thin layer of thermally conducting grease (Apiezon T). Current was passed through the slide to heat it, and the temperature was monitored with a thermocouple cemented to the surface of the slide near the sample. Measurements were at ~20°C intervals from room temperature to ~250°C. Cell constants were refined for the single-phase samples using 15–30 reflections with $2\theta \leq 120°$.

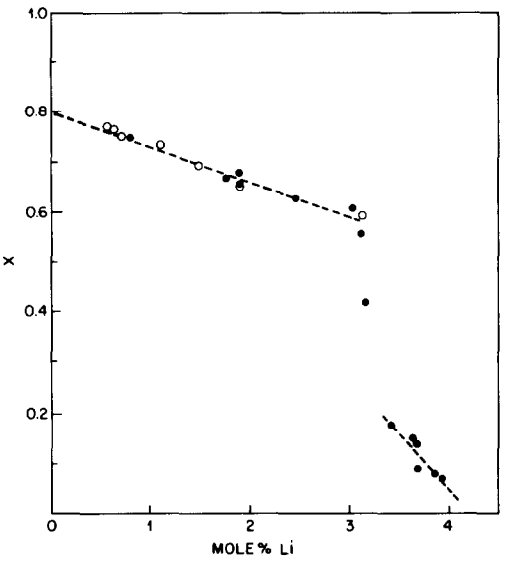

FIG. 1. x in $Li_{1-x}H_xNbO_3$ as a function of melt composition in benzoic acid/lithium benzoate melts at 250°. Closed circles represent stoichiometric samples (data from Ref. (*4*)); open circles congruent (nonstoichiometric) samples.

Thermal analysis. Thermogravimetric analysis (TGA) and differential scanning calorimetry (DSC) were performed on a Dupont 1090 Thermal Analysis System. Sample sizes were approximately 50 mg for TGA and 20 mg for DSC. Scan rates were 10°/min heating and 2°/min cooling.

Infrared spectroscopy. IR spectra were measured on pressed pellets containing ~5 wt% sample dispersed in AgBr. A Nicolet FTIR spectrometer was used.

Results and Discussion

The experimental results show evidence for a number of different exchanged phases as a function of composition and temperature. The stoichiometric and congruent systems will be discussed separately. A detailed analysis of the stoichiometric

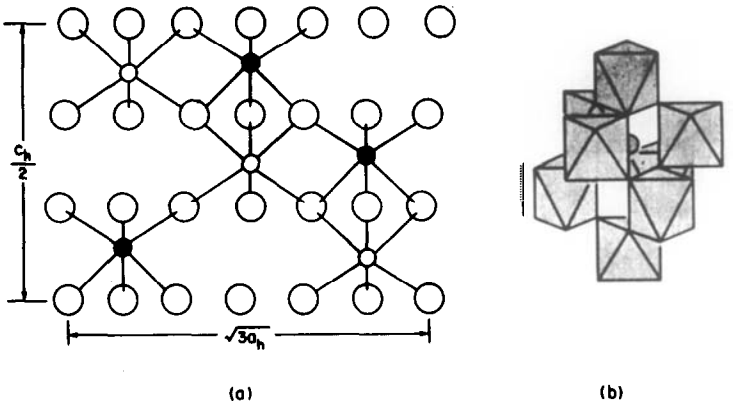

FIG. 2. Two views of the $LiNbO_3$ structure. (a) A projection of the $LiNbO_3$ structure on a plane perpendicular to the ⟨110⟩ direction. The small open circles represent lithiums, the small filled circles niobiums, and the large open circles oxygens. (b) A perspective view of the unique part of the $LiNbO_3$ structure with c_h approximately vertical. The octahedra represent NbO_6 units, and the small hatched circle is a lithium atom.

materials will be presented first; discussion of the congruent system will focus on the differences in behavior due to the stoichiometry of the $LiNbO_3$ starting material.

Stoichiometric $Li_{1-x}H_xNbO_3$

Structural results. For $0 \leq x \leq 0.12$ in $Li_{1-x}H_xNbO_3$, samples were single phase with the rhombohedral $LiNbO_3$ structure (Fig. 2). This phase is designated α-$Li_{1-x}H_xNbO_3$. A plot of cell constants (hexagonal form) vs x for this phase is shown in Fig. 3. As reported previously (*4*), the cell parameters show very little concentration dependence. No unusual structure changes with temperature were noted over the range studied.

The range from $0.12 < x < 0.55$ is a two-phase region. The next concentration interval, $0.55 \leq x \leq 0.75$, also gives single-phase samples with the rhombohedral $LiNbO_3$ structure. (Samples in this range will collectively be called β-$Li_{1-x}H_xNbO_3$.) However, these materials show quite complex structural behavior, both as a function of composition and temperature. A plot of cell parameters vs temperature for samples with $x = 0.56$, 0.63, 0.66, 0.72, and 0.75 is shown in Fig. 4. For $x = 0.56$, the room-temperature value of c_h is approximately the same as that in unexchanged $LiNbO_3$ (or α-$Li_{1-x}H_xNbO_3$), but a_h is considerably larger. As

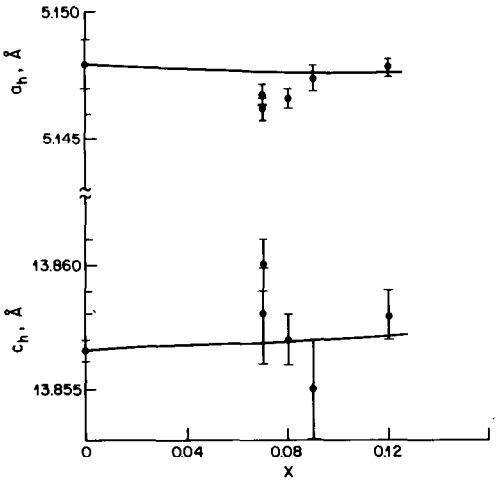

FIG. 3. Hexagonal unit cell parameters vs x in stoichiometric α-$Li_{1-x}H_xNbO_3$ (from Ref. (*4*)). Error bars shown are one σ.

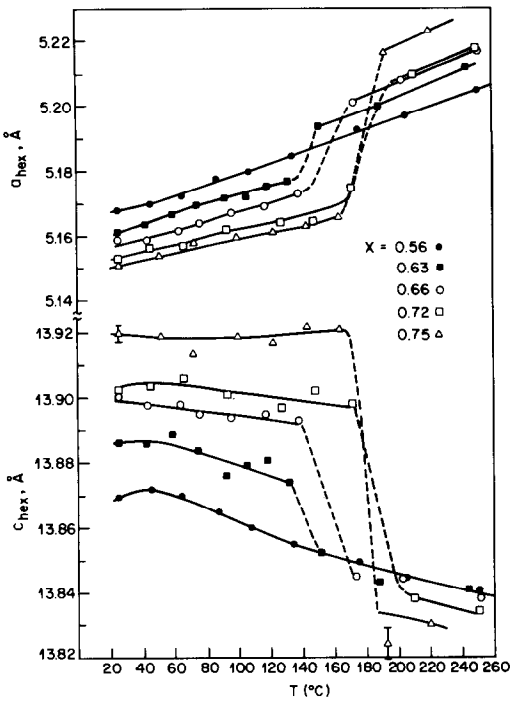

FIG. 4. Cell parameters as a function of temperature for stoichiometric β-$Li_{1-x}H_xNbO_3$ with $x = 0.56$, 0.63, 0.66, 0.72, and 0.75.

this compound is heated, both a_h and c_h increase initially. At ~60–100°C there is a change in slope of the cell parameter vs temperature plot; after this point, a_h increases more sharply, while c_h begins to decrease with rising temperature. This is a continuous transition, which shows up clearly in the DSC data for this composition (see below). For $x = 0.63$ at room temperature (in equilibrated samples), a_h is smaller than that for $x = 0.56$, while c_h is larger. As this composition is heated, its cell parameter vs temperature plots run roughly parallel to those for $x = 0.56$ until ~140°C. At this point a discontinuity in cell constants occurs; a_h increases to a value greater than that for $x = 0.56$ for this temperature, while c_h decreases to about the same value as for the lower concentration. Above this point the cell parameters again parallel the $x = 0.56$ plot. The discontinuity is a first-order structural transition. At higher values of x, the room temperature (equilibrium) value of a_h becomes progressively smaller with increasing x, while c_h increases. The plots of the cell constants vs temperature for $x = 0.66$, 0.72, and 0.75 run roughly parallel to those for $x = 0.56$ and 0.63. As x increases, the lower temperature gradual transition becomes more and more indistinct, while the high-temperature transition increases in magnitude and moves to higher temperatures.

The cell constants of $Li_{0.44}H_{0.56}NbO_3$ show no hysteresis with temperature. For the samples with x from 0.63 to 0.75, no hysteresis is observed if the temperature is cycled in the range below the high-temperature transition. This first-order transition shows considerable hysteresis, however, and when these samples are heated above the transition temperature and cooled rapidly, they remain in the high-temperature phase for a period of weeks to months. Figure 5 shows plots of cell constants vs x for the room temperature equilibrium phase, the metastable quenched phase, and at 220°C. This metastability of the high-temperature phase was reported in Ref. (*4*). One additional complication not noticed in the earlier study is the quenching behavior of $Li_{0.25}H_{0.75}NbO_3$: this composition shows two different quenched phases on rapid cooling. The first is metastable at room temperature for only a few hours (and cannot be seen at all if the sample is not cooled fast enough), while the second, which evolves from the first, remains at room temperature for about 2 weeks before reverting to the low-temperature phase. In Fig. 5, the initially observed metastable form of $Li_{0.25}H_{0.75}NbO_3$ is labeled 1, and the form observed second is labeled 2.

The composition range from $0.75 < x < 1.0$ is a two-phase region, where cubic $HNbO_3$ coexists with the various forms of β-$Li_{1-x}H_xNbO_3$.

Thermal measurements. Thermogravi-

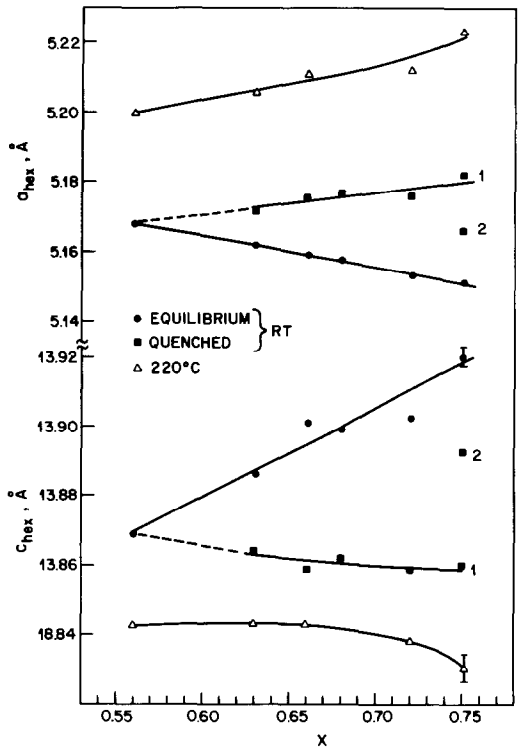

FIG. 5. Cell parameters vs x in stoichiometric β-$Li_{1-x}H_xNbO_3$: (●), room temperature equilibrium phase; square points, metastable phase, quenched from 200°C to room temperature; (△), measured at 220°C. The first and second metastable forms of $Li_{0.25}H_{0.75}NbO_3$ are labeled 1 and 2, respectively.

metric analysis (TGA) results were very similar for all rhombohedral $Li_{1-x}H_xNbO_3$ samples: all decomposed, giving off water, at approximately 350–500°C. A typical trace is shown in Fig. 6. The two-phase samples containing $HNbO_3$ showed an additional weight loss at ~250°C from the decomposition of this compound. Samples heated just above the decomposition temperature appeared amorphous to X rays. Prolonged heating at higher temperatures (>800°C) gave mixtures of $LiNbO_3$, $LiNb_3O_8$, and/or Nb_2O_5 depending on the value of x.

Differential scanning calorimetry (DSC) measurements of $Li_{1-x}H_xNbO_3$ samples with $x \leq 0.12$ were featureless up to the decomposition temperature. Samples with $0.56 \leq x \leq 0.75$ showed a number of endothermic peaks corresponding to the structural transitions outlined above. DSC traces for these samples taken on heating are shown in Fig. 7. For $x = 0.56$ a single, fairly broad peak is observed with an onset of ~80°C. This occurs over the temperature range of the gradual structural change seen in this material. Although this transition appears to be continuous, the considerable heat absorption involved argues against it being a strictly second-order transition. At $x = 0.63$ one sees this peak and evidence for a second peak, incompletely resolved from the first. For $x = 0.66$ there are two clearly resolved peaks at 80 and 130°C. At progressively higher proton concentrations the lower temperature peak flattens out while the other becomes sharper and greater in magnitude, and moves to higher temperatures. At $x = 0.72$ a small additional endothermic peak appears at ~175°C; at $x = 0.75$ this new peak has become equal in magnitude to the other high-temperature peak. Thus $Li_{1-x}H_xNbO_3$ with

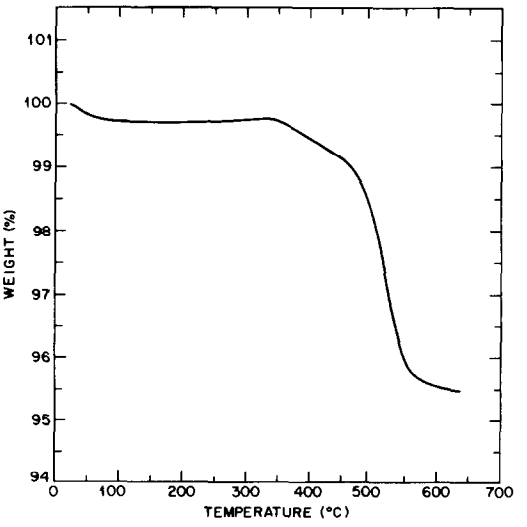

FIG. 6. Thermogravimetric analysis data for $Li_{0.25}H_{0.75}NbO_3$. The heating rate was 10°/min.

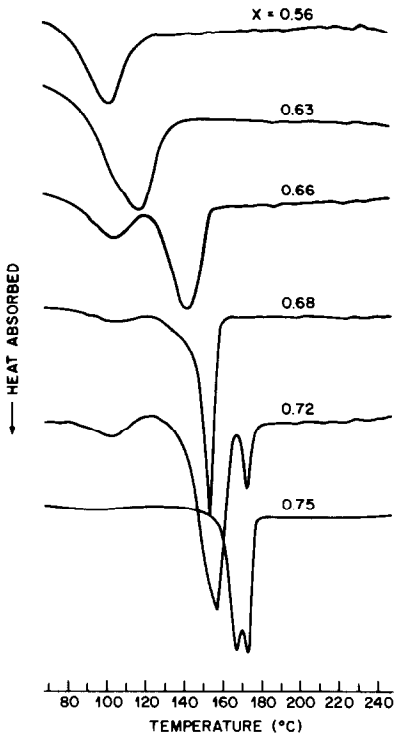

FIG. 7. Differential scanning calorimetry (DSC) data for stoichiometric β-$Li_{1-x}H_xNbO_3$.

$0.72 \leq x \leq 0.75$ actually has two closely spaced high-temperature transitions. The small temperature interval over which the intermediate phase is seen explains why it was not observed in the high-temperature X-ray measurements. The observation of two metastable forms of $Li_{0.25}H_{0.75}NbO_3$, however, attests to the existence of this intermediate phase.

For $Li_{1-x}H_xNbO_3$ samples showing endothermic peaks on heating, DSC measurements were also taken on cooling from 200°C to room temperature. However, in most cases no exothermic peaks could be seen due to the hysteresis of the high-temperature first-order transition. $Li_{0.25}H_{0.75}NbO_3$ was an exception; for this composition the hysteresis of the high-temperature transitions is small enough that evidence for both transitions could be seen as exothermic peaks at 120 and 100°C on cooling at 2°C/min. This sample could be cycled repeatedly through this temperature range with no change in the DSC trace. Samples with lower x were too sluggish to cycle continuously; to reproduce the DSC trace taken on heating, these had to be held at room temperature long enough to relax to the low-temperature phase. On the other hand, samples cycled through only the low-temperature gradual transition behaved reproducibly, although the transition was not clearly visible on cooling due to difficulty in achieving a high enough cooling rate in this temperature range.

The apparent differences between the transition temperatures observed by X-ray diffraction and DSC measurements should be addressed. These differences probably arise from two sources: first, from the fact that the diffraction was done at constant temperature, while the thermal measurements were taken with the temperature changing continuously; and second, because there may have been a small difference between the temperature at the sample position and at the thermocouple on the X-ray heater. In either case, the transition temperatures reported should be regarded as approximate.

From these structural and thermal measurements a phase diagram for the stoichiometric $Li_{1-x}H_xNbO_3$ system can be constructed, shown in Fig. 8. This diagram contains some revisions from the one proposed in Ref. (*4*), since at that time high-temperature diffraction data and thermal analysis data were not available. At lowest proton concentrations ($x \leq 0.12$), one sees the continuous solid solution α-$Li_{1-x}H_xNbO_3$. α coexists with β in the range from $0.12 < x < 0.56$. β-$Li_{1-x}H_xNbO_3$ is found from $0.56 \leq x \leq 0.75$. (In our previous study (*4*), where only room-temperature data were collected, two phases (β and γ) were proposed for this region; we now identify four rhombohedral phases, which

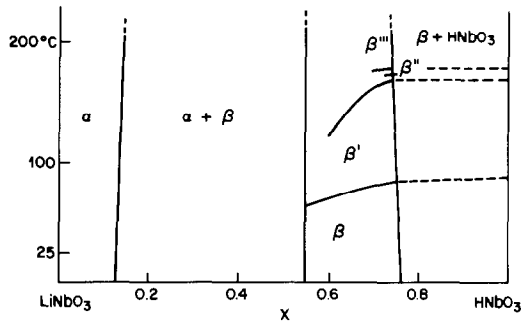

FIG. 8. An approximate phase diagram for the stoichiometric $LiNbO_3$–$HNbO_3$ system.

we choose to call β, β', β'', and β'''.) From $0.75 < x < 1.0$, rhombohedral β-$Li_{1-x}H_xNbO_3$ coexists with cubic $HNbO_3$.

The fact that the lower limit of stability for the β phase is close to $x = 0.5$ is suggestive of some form of ordering between lithium and proton sites. This could occur without the introduction of a superstructure, simply by a lowering of symmetry. For example, making the two lithium sites in the $LiNbO_3$ structure (*5*) along the c_h axis inequivalent would lower the space group symmetry from $R3c$ to $R3$ without changing the size of the unit cell. This kind of ordering could only be detected by analyzing the diffracted intensities to reveal the cell contents.

Looking more closely at the stability range for the various forms of β-$Li_{1-x}H_xNbO_3$, complicated and unusual behavior is seen. As x increases from 0.56 to 0.75, one sees first one structural transition, then two, and finally three. The question arises of how to draw the phase diagram in such a region where all members of the series clearly belong to the same solid solution phase at high temperature, but show different numbers of phase transitions on cooling. For example, should the first-order transition which is seen for $x = 0.63$ be assumed also to exist for $x = 0.56$, but be too small in magnitude or too sluggish to observe? Or does the transition simply vanish? The data in Fig. 5 support the latter possibility. The differences between the cell constants of the room-temperature equilibrium phase and the metastable phase produced by quenching diminish as x decreases from 0.75 to 0.63. At $x = 0.56$, the extrapolations of the plots of a_h and c_h vs x for the metastable phase intersect those of the equilibrium phase. Thus it would appear that this transition does not occur for $x = 0.56$, and that the system exhibits critical behavior, with a critical point at approximately $x = 0.56$, $T = 120$°C. It is also possible that this transition drops off toward zero temperature at $x = 0.56$, rather than terminating in a point at 120°. To do this, it would have to cross over the gradual transition, but this is quite possible since the two transitions do not appear to be related. (For example, in quenched samples of $Li_{0.37}H_{0.63}NbO_3$, the lower temperature, continuous transition can be seen in the DSC data on heating even though the material is in the high-temperature metastable form.) Without more data at x slightly greater than 0.56, it is not possible to choose between these two possibilities. Therefore the transition is shown in the phase diagram where it is observed, with no attempt to predict its behavior where it is not seen.

There are fewer data which can shed light on the nature of the third transition which is observed for $x \geq 0.72$. It seems probable, though, that the onset of this transition represents a second critical point at $x \approx 0.70$, $T \approx 150$°C. In this case it is not possible for the high-temperature first-order transition to fall off to low temperatures, because to do so it would have to cross over the lower first-order transition, and in this case these transitions are related. Therefore the transitions in β-$Li_{1-x}H_xNbO_3$ are described in the following way: At the high end of its range ($0.72 \leq x \leq 0.75$), β-$Li_{1-x}H_xNbO_3$ undergoes a continuous transition to β' at ~60°C. β' then transforms to β'' and β''' in two closely spaced first-order transitions at ~160–175°C. When x becomes less than

0.72, the higher temperature first-order transition decreases in magnitude and disappears. Thus the distinction between β'' and β''' is lost. At $x < 0.63$, the other first-order transition also drops out, leaving β', β'' and β''' indistinguishable in this concentration range.

In the absence of more complete structural information for the β-$Li_{1-x}H_xNbO_3$ system, it is not possible to determine a unique microscopic model for the phase transitions observed. It seems likely, however, that some form of proton ordering is involved. Further measurements more sensitive to protons and lithium ions, particularly neutron diffraction and nmr, will be necessary to obtain a detailed understanding of this system's unusual behavior.

Infrared spectroscopic results. Infrared spectra in the OH stretching region are shown in Fig. 9 for a variety of stoichiometric $Li_{1-x}H_xNbO_3$ samples. Note that in the α-$Li_{1-x}H_xNbO_3$ range ($0 < x \leq 0.12$) the IR spectra show more complicated behavior than was observed by X-ray diffraction. In the samples with $x = 0.07$ and 0.09 (Figs. 9a and b), two closely spaced OH absorptions are observed at 3480 and 3510 cm^{-1}. As x increases, the higher energy peak gains intensity with respect to the lower energy one. This shows that there are two distinct but very similar proton sites in this material, and that the site corresponding to the 3480-cm^{-1} peak is filled first. The peak at 3480 cm^{-1} is at the same position as that observed in single crystals having very small proton concentrations, whether from small amounts of water vapor incorporated during crystal growth or poling, or from proton exchange at the surface followed by lengthy annealing. The variation in the areas of the peaks with x indicates that this first site is filled at $x \approx 0.04$. As x increases to 0.12 (Fig. 9c), a single OH absorption peak is observed at 3510 cm^{-1}. The width at half maximum of this peak is approximately the same as that of the 3510-cm^{-1} peak in

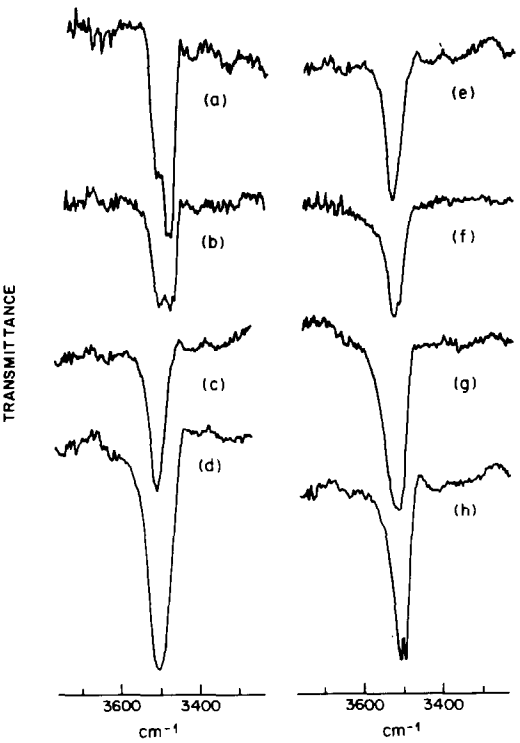

FIG. 9. Infrared spectra in the OH stretching region for stoichiometric $Li_{1-x}H_xNbO_3$ with x = (a) 0.07; (b) 0.09; (c) 0.12; (d) 0.56; (e) 0.72 (quenched from 200°C to room temperature); (f) 0.72 (room-temperature equilibrium phase); (g) 0.75 (quenched); (h) 0.75 (room-temperature phase).

the $x = 0.07$ and 0.09 samples. Thus it appears that the proton site corresponding to the 3480-cm^{-1} peak empties as the 3510-cm^{-1} site fills, so that at $x = 0.12$ only the latter type of proton site is occupied.

Additional information about the nature of the proton site in α-$Li_{1-x}H_xNbO_3$ can be inferred from infrared measurements on single crystals. When congruent $LiNbO_3$ crystals are exchanged under conditions giving a surface x in the α-$Li_{1-x}H_xNbO_3$ range, their IR spectra in unpolarized light look the same as those in Fig. 9. (As will be discussed below, the behavior of stoichiometric and congruent $Li_{1-x}H_xNbO_3$ is very similar in this concentration range. The appearance of a new phase in the congruent

system, however, makes comparisons invalid at higher values of x). In polarized light, however, a maximum in intensity is seen for $\mathbf{E} \perp c_h$, while the absorption is extinguished for $\mathbf{E} \parallel c_h$. This means that the O–H vector must be perpendicular to the c_h axis. Thus the proton sites must lie within the (approximately) hexagonally closest packed oxide layers in the $LiNbO_3$ structure, rather than in metal ion-like sites between layers. This same conclusion was reached by Herrington *et al.* (*6*) (they concluded that the O–H vector must be perpendicular to $c_h \pm 5°$) in a spectroscopic study of $LiNbO_3$ crystals which had incorporated water by being annealed at high temperature in a wet atmosphere. The IR spectrum for $Li_{0.44}H_{0.56}NbO_3$ (Fig. 9d) shows a single OH absorption whose maximum is at the same position as seen for $Li_{0.88}H_{0.12}NbO_3$ (3510 cm^{-1}); however, the peak width is noticeably greater. This suggests the presence of a distribution of proton sites in $Li_{0.44}H_{0.56}NbO_3$ having slightly different environments. For $0.63 \leq x \leq 0.75$, IR spectra of samples quenched from 200°C to room temperature resemble the spectrum of $Li_{0.44}H_{0.56}NbO_3$ (Figs. 9e and g). Samples which are in the equilibrium room-temperature phase, however, show a somewhat narrower OH absorption peak centered at 3510 cm^{-1}, but also have an additional sharp peak at 3495 cm^{-1} (Figs. 9f and h). The intensity of this new peak with respect to the 3510 cm^{-1} one increases with increasing x, until the two peaks have roughly comparable magnitudes when $x = 0.75$.

IR spectra could not be obtained at high temperatures because the AgBr in the pellets darkened when heated, resulting in poor optical quality. Pellets of quenched samples were made by heating and quenching the $Li_{1-x}H_xNbO_3$ powder, then fabricating the pellet. Similarly, equilibrium phase pellets were made by converting the material to the low-temperature phase before pelletizing. X-ray diffraction measurements on the pellets confirmed the presence of the desired phase.

The IR spectrum of $HNbO_3$ (Fig. 10) is very different from those of the partially exchanged compounds. Its OH absorption peak is much broader, and is shifted to lower energy (centered at 3300 cm^{-1}). This kind of shift and broadening is typical of hydrogen-bonded systems.

Congruent $Li_{1-x}H_xNbO_3$

The dependence of x in $Li_{1-x}H_xNbO_3$ on the lithium concentration in benzoic acid melts (Fig. 1) does not appear to be much affected by the stoichiometry of the $LiNbO_3$ starting material. The structural behavior of congruent $Li_{1-x}H_xNbO_3$ was also found to be very similar to that of stoichiometric material up to $x = 0.68$. For α-$Li_{1-x}H_xNbO_3$, the evidence is indirect, because the diffusion coefficient for the proton exchange reaction becomes too low in this concentration range to achieve full reaction in a reasonable time for the particle size used (20 μ). In a different study (*7*), congruent $LiNbO_3$ crystals were subjected

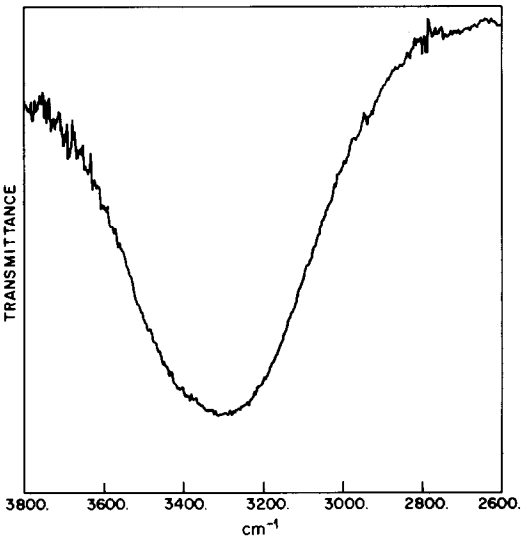

FIG. 10. The infrared spectrum of $HNbO_3$.

to proton exchange in benzoic acid/lithium benzoate melts of varying composition. This produced exchanged layers at the surface of the crystals which were studied by prism coupling (giving the refractive index depth profile) and IR spectroscopy. Comparison of these results with those for stoichiometric $Li_{1-x}H_xNbO_3$ powders shows that the boundaries of the α–β two-phase region and the spectroscopic details in the α-$Li_{1-x}H_xNbO_3$ concentration range are essentially independent of stoichiometry. Congruent β-$Li_{1-x}H_xNbO_3$ powder samples with $x = 0.59$ and 0.65 had room temperature cell constants (both equilibrium phase and quenched) indistinguishable from their stoichiometric counterparts with the same x; IR spectra were also quite similar. DSC measurements showed the same features, with the phase transitions occurring approximately 10°C lower for the congruent materials.

Samples with $x = 0.68$ and 0.73 were two phase: the rhombohedral β phase plus a new monoclinic phase (discussed in detail below). For $x = 0.75$ and 0.77, samples were single phase with a monoclinic structure, and gave no evidence of any phase transitions in their DSC data. A mixture of the monoclinic phase and cubic $HNbO_3$ was observed for $x > 0.77$. $HNbO_3$ prepared from congruent $LiNbO_3$ was not distinguishable by X rays or IR from that prepared using stoichiometric starting material.

Monoclinic $Li_{1-x}H_xNbO_3$. An exchanged phase with a new structure was found for $x = 0.75$ to 0.77. It was fit with a monoclinic cell: $a = 8.906(3)$, $b = 5.191(3)$, $c = 13.944(8)$ Å, $\beta = 90.77(5)°$ for $x = 0.77$, and approximately the same for $x = 0.75$. The observed d spacings and X-ray intensities for monoclinic $Li_{0.23}H_{0.77}NbO_3$ are shown in Table I. This monoclinic cell is related to the hexagonal $LiNbO_3$ cell by the relations: $a_{mono} \simeq [1\bar{2}0]_h$, $b_{mono} \simeq a_h$, $c_{mono} \simeq c_h$. This phase has the same structure as MnF_3(8) ($a = 8.904(3)$, $b = 5.037(2)$, $c = 13.448(5)$ Å, $\beta = 92.74(4)°$), and is only the second reported example of this structure type. In the case of MnF_3, the distortions from rhombohedral symmetry were attributed to Jahn-Teller effects. In monoclinic $Li_{1-x}H_xNbO_3$, they are probably due to hydrogen-bonding interactions.

TABLE I

DIFFRACTION PATTERN FOR CONGRUENT $Li_{0.23}H_{0.77}NbO_3$

$h\ k\ l$	$2\theta_{obs}$ (°)	d (Å)	I/I_0
$\bar{1}\ 1\ 2$	23.52	3.779	100
$2\ 1\ 2$	29.46	3.029	3
$\bar{1}\ 1\ 4$	32.44	2.758	10
$\bar{1}\ 0\ 5$	33.52	2.671	30
$0\ 2\ 0$	34.48	2.599	2
$0\ 0\ 6$	38.72	2.324	2
$\bar{3}\ 1\ 3$	39.82	2.262	10
$\bar{2}\ 2\ 2$	42.24	2.148	10
$2\ 2\ 2$	42.42	2.129	2
$\bar{4}\ 0\ 4$	48.16	1.888	17
$\bar{5}\ 0\ 1$	51.56	1.771	1
$\bar{3}\ 1\ 6$	52.72	1.735	5
$\bar{2}\ 1\ 7$	53.12	1.723	5
$1\ 0\ 8$	53.68	1.706	1
$4\ 2\ 0$	54.26	1.689	10
$5\ 1\ 0$	54.42	1.684	2
$0\ 1\ 8$	55.54	1.653	5
$\bar{1}\ 2\ 7$	59.20	1.559	4
$\bar{2}\ 1\ 8$	59.34	1.556	6
$\bar{5}\ 1\ 4$	60.68	1.525	2
$4\ 2\ 4$	61.16	1.514	2
$\bar{1}\ 1\ 10$	70.60	1.333	2

In a previous paper, we mentioned an unexplained, weak X-ray peak which was observed in stoichiometric $Li_{1-x}H_xNbO_3$ samples at high values of x. This peak is now seen to be due to the intense $(\bar{1}05)$ reflection of monoclinic $Li_{1-x}H_xNbO_3$, which must arise from the presence of a trace of congruent $LiNbO_3$ in the starting material.

The infrared spectrum of monoclinic $Li_{0.23}H_{0.77}NbO_3$ is shown in Fig. 11. Interestingly, this spectrum contains features of both rhombohedral $Li_{1-x}H_xNbO_3$ and cubic $HNbO_3$. It shows a sharp, intense OH ab-

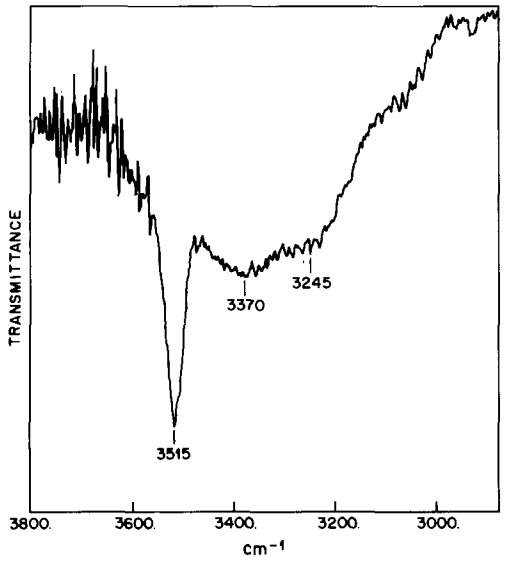

FIG. 11. The infrared spectrum of congruent monoclinic $Li_{0.23}H_{0.77}NbO_3$.

sorption at 3515 cm^{-1}, and broader peaks at approximately 3370 cm^{-1} and 3240 cm^{-1}. Thus this phase appears to have proton sites similar to those in rhombohedral $Li_{1-x}H_xNbO_3$, plus some additional sites involving hydrogen bonding.

Refractive index changes. One very intriguing question raised by this system concerns the origin of the refractive index changes caused by proton exchange. Previous studies (*7, 9*) have shown that all the index changes (+0.12 for n_e, −0.05 for n_o at 633 nm) occur in the concentration range $x < 0.10$, that is, in α-$Li_{1-x}H_xNbO_3$. This phase shows no significant changes in cell parameters as a function of x. Thus one has large index changes which are not associated with any change in volume, nor with the addition of highly polarizable ions (both Li^+ and H^+ have very small polarizabilities). What, then, causes the index changes? It is proposed that the answer lies in the difference in site preference of H^+ and Li^+. IR spectra on single crystals showed that the protons in α-$Li_{1-x}H_xNbO_3$ are located within the oxide planes, replacing lithium ions which were in octahedral sites between those planes. Thus the replacement of a lithium ion with a proton results in a displacement of positive charge along c_h, moving charge away from one triangular face of the octahedral site and into the opposite face. This might be expected to increase the polarizability of the oxygens more distant from the proton, while decreasing the polarizability of the closer oxygens. Such a model would explain why n_e (along c_h) increases on proton exchange while n_o (perpendicular to c_h) decreases.

This hypothesis makes it possible to predict the effects of proton substitution on the optical properties of other materials. In any system where a proton replaces a metal ion in an octahedral or tetrahedral site, the proton will tend to locate well off center in the site since it prefers a smaller coordination number (two or three) and shorter contacts to anions. Thus in any such material where the proton locates in one preferred position in the octahedron or tetrahedron (rather than a random distribution), one should expect to see anisotropic changes in the refractive indices.

Conclusions

The $Li_{1-x}H_xNbO_3$ system clearly exhibits a complex structural chemistry. A number of distinct phases have been observed, along with a variety of phase transitions. Two of these are discontinuous transitions and appear to show critical behavior, while a third transition is continuous in nature. While present data are not sufficient to define a unique model for this system, an order–disorder mechanism for the transitions seems likely. These complicated structural changes, all occurring at high proton concentrations, underscore the conclusion that proton exchanged waveguides should be fabricated in the low proton concentration (α-$Li_{1-x}H_xNbO_3$) range.

The congruent $Li_{1-x}H_xNbO_3$ system was

found to behave similarly to the stoichiometric material in most respects. The most notable exception is the observation of the new monoclinic phase at high values of x. The existence of this distorted phase may explain the observation of surface damage in certain orientations on congruent $LiNbO_3$ crystals exchanged in straight benzoic acid.

The results of this study have been used to propose a model for the refractive index changes brought on by proton exchange in $LiNbO_3$. This model can possibly be used to predict the optical effects of proton exchange in other systems.

Acknowledgments

Thanks are due to R. J. Cava, P. K. Gallagher, M. E. Lines, P. B. Littlewood, D. W. Murphy, R. R. Roth, and S. C. Abrahams for helpful discussions.

References

1. C. E. Rice and J. L. Jackel, *J. Solid State Chem.* **41,** 308 (1982).
2. J. L. Jackel, C. E. Rice, and J. J. Veselka, *Appl. Phys. Lett.* **41,** 607 (1982).
3. (*a*) J. L. Jackel, C. E. Rice, and J. J. Veselka, *Electronics Lett.* **19,** 387 (1983); (*b*) A. Yi-Yan, *Appl. Phys. Lett.* **42,** 633 (1983); (*c*) J. L. Jackel, A. M. Glass, G. E. Peterson, C. E. Rice, D. H. Olson, and J. J. Veselka, *J. Appl. Phys.* **55,** 269 (1984); (*d*) M. de Micheli, J. Botineau, S. Neveu, T. Sibillot, D. D. Ostrowsky, and M. Papuchon, *Optics Lett.* **8,** 116 (1983).
4. C. E. Rice and J. L. Jackel, *Mat. Res. Bull.* **19,** 591 (1984).
5. S. C. Abrahams, J. M. Reddy, and J. L. Bernstein, *J. Phys. Chem. Solids* **27,** 997 (1966).
6. J. R. Herrington, B. Dischler, A. Rauber, and J. Schneider, *Solid State Commun.* **12,** 351 (1973).
7. J. L. Jackel and C. E. Rice, Proc., 7th Intl. Meeting on Integrated and Guided Wave Optics, Kissimmee, Fla., 1984.
8. M. A. Hepworth and K. H. Jack, *Acta Crystallogr.* **10,** 345 (1957).
9. C. E. Rice, J. L. Jackel, and W. L. Brown, *J. Appl. Phys.* **57,** 4437 (1985).